PAPER

Check for updates

Interaction between carbon dots from folic acid and their cellular receptor: a qualitative physicochemical approach†

Erika Adhel,[a] Nguyêt-Thanh Ha Duong, [ID][a] Thi Huyen Vu,[b] Dario Taverna,[c] Souad Ammar [ID][a] and Nawal Serradji [ID]*[a]

According to the World Health Organization, the number of cancers (all cancers, both sexes, all ages and worldwide) in 2020 reached a total of 19 292 789 new cases leading to 9 958 133 deaths during the same period. Many cancers could be cured if detected early. Preventing cancer and detecting it early are two essential strategies for controlling this pathology. For this purpose, several strategies have been described for imaging cancer cells. One of them is based on the use of carbon nanoparticles called carbon dots, tools of physical chemistry. The literature describes that cancer cells can be imaged using carbon dots obtained from folic acid and that the *in cellulo* observed photoluminescence probably results from the interaction of these nanoparticles with the folic acid–receptor, a cell surface protein overexpressed in many malignant cells. However, this interaction has never been directly demonstrated yet. We investigated it, for the first time, using (i) freshly synthesized and fully characterized carbon dots, (ii) folate binding protein, a folic acid–receptor model protein and (iii) fluorescence spectroscopy and isothermal titration calorimetry, two powerful methods for detecting molecular interactions. Our results even highlight a selective interaction between these carbon made nano-objects and their biological target.

Introduction

Targeted, and therefore selective, drug delivery is now a major therapeutic issue in medicine. Indeed, this strategy enhances the performance of the drugs administered while drastically reducing their side effects, often related to their recognition by multiple possible biological targets.

Cancer is an example of a pathology requiring a targeted chemotherapeutic approach. With approximately 10 million deaths per year, cancer is the second leading cause of death in the world. Almost one in six deaths is due to cancer worldwide. It is therefore imperative to offer additional tools to attempt strict control of this pathology. Increasing the efficacy of pre-existing cytotoxic compounds and diminishing induced side effects appear as relevant strategies. To improve drug efficiency, biological therapy,[1] photodynamic therapy[2] or dietary interventions[3] can be used. To reduce side effects, directing drugs to receptors selectively overexpressed by cancer cells can be exploited. The interaction between folic acid receptor (FA-R)[4] and folic acid (FA), its natural ligand, is a good illustration of such a therapeutic pathway.[5,6] Indeed, FA is highly tolerant to chemical modifications and its recognition by its receptor is seldom altered, making FA-R-overexpressing cancer cell targeting[7] and, consequently, drug-conjugate endocytosis and fast cell penetration highly relevant.

In parallel, there is much interest in the use of nanoparticles (NPs) in therapy, due to their numerous advantages: nanometer size, concentration of the drug on their surface, protection of the latter against enzymatic degradation and so on. Therapeutic NPs are of varied natures.[8] Among them, Carbon Dots (CDs) are emerging as metal-free NPs with remarkable intrinsic optical properties.[9] They were discovered accidentally in 2004 by Xu *et al.*[10] and since then, a variety of easy in-solution synthesis methods have been developed.[11] Most CDs exhibit blue-green emissions. Nowadays, they are typically green substitutes for the previous toxic CdSe quantum dots (QDs).[12] Their building block is made out of carbon[13] with some doped light heteroatoms, creating NPs that are more biocompatible, soluble in water and less toxic than QDs.[14] Moreover, surface functionalization of CDs is easy, using their surface sp[3] carbon atoms.[15]

[a] *Université Paris Cité, CNRS, ITODYS, F-75013 Paris, France. E-mail: serradji@u-paris.fr; Fax: +33 1 57277263; Tel: +33 1 57278883*

[b] *University of Engineering and Technology, Vietnam National University, Hanoi (VNUH), Vietnam*

[c] *Sorbonne Université, CNRS, IMPMC, F-75005 Paris, France*

† Electronic supplementary information (ESI) available. See DOI: https://doi.org/10.1039/d3cp01277h

Thanks to these unique properties, the number of related publications about their syntheses, properties and biomedical applications increases exponentially every year.[16–18] Despite this huge scientific effervescence, the exact nature of these CDs is still a subject of discussion. For instance, carbon nitride C_3N_4,[19] nanographene, nanographene oxide[20] and semiconducting polymeric CDs have been described and named CDs in the literature.[21] Furthermore, the understanding of the key factors controlling their physicochemical properties remains challenging. Zhu *et al.* proposed that some properties, *e.g.* toxicity, would be dictated primarily by the CD core, while other properties, *e.g.* dispersibility, would depend primarily on their surface functional groups.[22] Zhi *et al.* reviewed prevalent hypotheses regarding the origin of their photoluminescence, highlighting the role of the in-gap surface group energy levels in the radiative de-excitation processes of CDs assumed as semiconducting nanostructures.[23]

Their use as carriers for drug delivery, functionalizing their surface by specific biomolecules such as FA, and the mechanism of their interaction with FA-R have been addressed.[24–33] Indeed, FA-R is able to interact with its natural ligand, but also with conjugates resulting from the covalent binding of FA to various organic groups. FA attached to larger entities, such as nanovehicles including polymers,[34] liposomes, proteins[35] or NPs, is also recognized by this receptor, illustrating its wide capacity for ligand recognition. Numerous studies, carried out on cell cultures and using different methods, make it possible to take advantage of the specificity of this ligand–receptor recognition without ever demonstrating a direct interaction. For instance, Narmani *et al.* reviewed NPs functionalized with FA and successfully prepared as drug delivery systems.[36] In addition, Yücel *et al.* grafted FA to methotrexate (a FA-R antagonist)-loaded gold NPs and demonstrated the receptor specificity of the conjugate by fluorescence microscopy imaging.[37] Butzbach *et al.* synthesized modified dextran NPs and conjugated them with FA in order to increase the uptake of a photosensitizer into tumour cells. A completion assay, using an excess of free FA, demonstrated that these NPs are recognized by FA-R.[38] CDs obtained by in-solution FA decomposition (CDs_{FA}) are able to detect or to image cells expressing FA-R, presumably through their interaction with this receptor, but this point was not established unambiguously.[39–41] These studies also pointed out the possibility of selectively imaging cancer cells using such CDs_{FA},[42] but did not provide spectroscopic data to validate this biological feature.

Therefore, for the first time in this work and according to the chemist's point of view, we used absorption, emission spectrophotometry methods and isothermal titration calorimetry to evidence the interaction between CDs_{FA} and a soluble form of FA-R, the bovine folate binding protein (bFBP), a surrogate of the human FA-R with 80% homology with the human form and also a high affinity for FA.[43] CDs_{FA} were produced by hydrothermal decomposition of FA and characterised. In addition, their putative selectivity was investigated using lactoferrin (LF), another FA target-protein.[44,45]

Experimental methods

Chemicals

Folic acid (FA), quinine sulfate monohydrate 90%, folate binding protein from bovine milk (bFBP), human lactoferrin (LF) and sodium azide 99% were purchased from Sigma-Aldrich, and potassium hydrogen phosphate trihydrate from Alfa Aesar. PURELAB Classic UV provided 18.2 MΩ cm ultra-pure type I Milli-Q water. Phosphate buffer solution was prepared by dissolving 20 mM of $K_2HPO_4 \cdot 3H_2O$ (Sigma) in Milli-Q water and adjusting the pH to 7.4 by addition of commercial 37% HCl solution (Sigma). The pH of the solution was measured on a Jenco pH meter, equipped with an Ingold microelectrode and referenced to standard buffers at pH = 7.0 and 10.0 (Sigma).

Hydrothermal synthesis and purification of CDs_{FA}

A suspension of FA (0.15 g) in Milli-Q water (50 mL) was placed in a beaker and homogenised by sonication for 20 minutes, in an ultrasonic bath (VWR Ultrasonic Cleaner). The resulting suspension was then transferred to a 120 mL Teflon chamber in a high-pressure reactor autoclave (302 AC T304 030317, Moline, Illinois, USA), and heated in a Serlabo SAV type oven for 6 hours at 180 °C. The autoclave was then cooled to room temperature. The yellow suspension obtained was filtered through a 0.22 μm syringe filter, dialysed 3 times (for 2 hours, overnight, and again for 2 hours) against Milli-Q water (molecular weight cut-off (MWCO) of 100–500 kDa for the Slide-A-Lyser, Thermo Scientific). Freeze-drying (Modulyo freeze dryer) led to 30 mg (20% w/w) of the resulting CDs_{FA} as a yellow powder, and stored in the dark under argon at −20 °C.

Preparation of stock solutions

For CDs_{FA} characterisation, the solutions were freshly prepared by dilution of a 1 mg mL^{-1} stock solution stored at +4 °C.

CDs_{FA} characterization

Dynamic light scattering (DLS) and zeta potential (ζ) measurements (Malvern-Zetasizer Nano ZS90) were performed in 3 mL plastic cuvettes with a 1 cm optical path and a folded capillary zeta cell, respectively. UV-Visible absorption spectra were recorded on CDs_{FA} and FA in Milli-Q water, at 25.0 ± 0.5 °C using a Cary 4000 spectrophotometer with a SUPRACIL quartz cuvette (1 × 1 cm). Fluorescence spectra of the same solutions were obtained, at 25.0 ± 0.5 °C, on a Fluorolog spectrophotometer, using a SUPRACIL quartz cuvette (1 × 1 cm). To quantify the quantum yield of CDs_{FA}, the optical absorption and fluorescence spectra of a reference quinine sulfate monohydrate aqueous solution were recorded.

Infrared (IR) absorption spectra were recorded on FA and CDs_{FA} (KBr method), using a VariGATRTM, USA, Thermo Scientific spectrometer (Class 1 Laser Product).

Transmission electron microscopy (TEM) and scanning transmission electron microscopy (STEM) data were acquired on a JEOL 2100F microscope, equipped with a Gatan GIF 2001 for electron energy loss spectroscopy (EELS) measurements. In STEM-EELS experiments, images were recorded using the

This journal is © the Owner Societies 2023

Phys. Chem. Chem. Phys., 2023, **25**, 14324–14333 | **14325**

following parameters: spectrum image size: 69 × 98 nm (21 × 30 pixels); spot size: 1 nm; energy dispersion: 0.5 eV per channel; dwell time: 0.3 sec per pixel. To complete these analyses, high-angle annular-dark-field (HAADF) imaging was performed on the same microscope. For all these experiments, a drop of the CDs_{FA} aqueous colloid was deposited on a holey carbon–Cu 300 mesh grid from Oxford Instruments.

X-ray photoelectron spectroscopy (XPS) was used to check the surface chemical composition of the particles produced. A K-Alpha$^+$ system (ThermoFisher Scientific, East Grinstead, UK) fitted with a micro-focused, monochromatic Al Kα X-ray source (1486.6 eV, spot size: 400 μm) was used. The survey spectra were collected in steps of 1 eV at a pass energy of 150 eV. They were calibrated against the (C–C/C–H) C 1s component set at 285 eV. High-resolution spectra of separate photoelectron signals (C, O, N) were taken by steps of 0.1 eV at a pass energy of 40 eV. A few milligrams of CDs_{FA} as powder were deposited on carbon tape to form a thick layer.

A high-resolution mass spectrum (HRMS) was recorded at the Small Molecule Mass Spectrometry platform of IMAGIF (Centre de Recherche de Gif – **https://www.imagif.cnrs.fr**), on a Waters spectrometer using electrospray ionization-TOF (ESI-TOF; M + H$^+$).

FA-R interaction

Absorption and fluorescence spectrophotometries. bFBP and LF solutions (50 μM) were stored at −20 °C in the following buffer: $K_2HPO_4 \cdot 3H_2O$ (20 mM) and NaCl (100 mM), pH = 7.4. For the interaction studies, ligands (10 μM of FA or 0.4 mg mL^{-1} of CDs_{FA}) and 0.5 μM of protein were dissolved in 20 mM phosphate buffer, pH = 7.4. The absorption and fluorescence spectra of the resulting mixture were recorded. Experiments were performed in triplicate. Note that CDs_{FA} concentrations are expressed in terms of mg mL^{-1}. OriginPro 7 and Microsoft Excel 2013 were used for data analysis and artwork.

Isothermal titration calorimetry. During isothermal titration calorimetry (ITC) experiments, proteins (FBP or lactoferrin) and ligands (CDs_{FA}) were dissolved in the same 20 mM phosphate buffer, pH 7.4. The experiments were carrying out using a NanoITC low volume calorimeter (TA instrument) with a gold cell and an active cell volume of 166 μL. All ITC titrations were performed at 25 °C, at a stirring rate of 150 rpm, using a titrating syringe volume of 50 μL. Typically, an initial injection of 1 μL was performed and followed by an automated sequence

of 24 injections of 2 μL of 0.11 mg mL^{-1} CDs_{FA} titrant into the sample cell containing 20 μM FBP, spaced at 300–600 min intervals (direct titration). The control experimentation involved injecting ligand (0.11 mg mL^{-1} CDs_{FA}) into the cell that contained the buffer alone. The direct titration experiments were performed in triplicate.

The reverse titration was also performed with the same automated sequence of injections wherein 50 μL of 100 μM FBP were loaded in the syringe and 8.55 μg mL^{-1} CDs_{FA} were in the cell. The reverse titration experiments were carried out in duplicate.

Data were collected automatically and analysed, after substitution of the heat produced during CDs_{FA} dilution, using the NanoAnalyze software from TA instruments and an independent binding site model to yield the association constant, stoichiometry, and the thermodynamic parameters (ΔH and ΔS) of binding reactions.

Results and discussion

Synthesis and characterisation of CDs_{FA}

CDs_{FA} were synthesised by a hydrothermal method using FA as the carbon source (Scheme 1).

We first tried to reproduce the synthesis proposed by Bhunia et al.[42] who described a simple one-step route, in which FA was mixed with sodium hydroxide and heated at 90 °C for 2 hours to induce carbonisation. However, our trials did not provide luminescent objects. We then modified the experimental procedure by increasing the temperature to 180 °C, without however obtaining CDs_{FA}. Finally, removing sodium hydroxide from the reaction medium and heating to 180 °C (Scheme 1) led to a yellow suspension with a fluorescent behaviour which is not observed in free FA under UV irradiation (Fig. 1). The product was purified by filtration through a 0.22 μm filter, dialysed against Milli-Q water and lyophilised to give the desired CDs_{FA} as a yellow powder. Running the reaction for 6 hours increased the yield to 20% whereas it was only 3.3% after 2 hours. We also improved particle purification by filtering before dialysis and by reducing the MWCO of the dialysis bag. CDs_{FA} obtained after a 6 hour reaction were selected for characterisation and interaction studies. Data concerning size, morphology, zeta potential, composition and/or surface analysis of the nanoparticles are presented in the ESI.†

The complementarity results obtained from EELS, XPS and FTIR experiments, presented in the ESI,† allow us to propose that (i) the sample consists of carbon, nitrogen and oxygen,
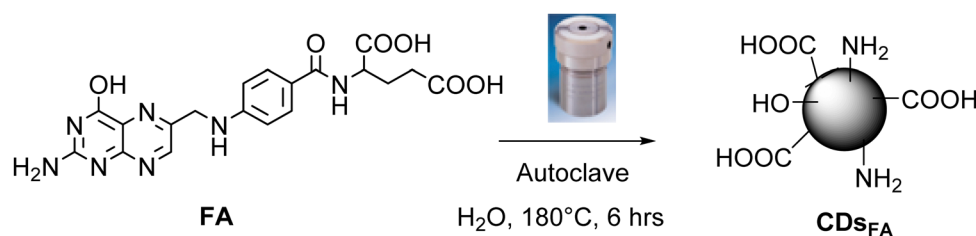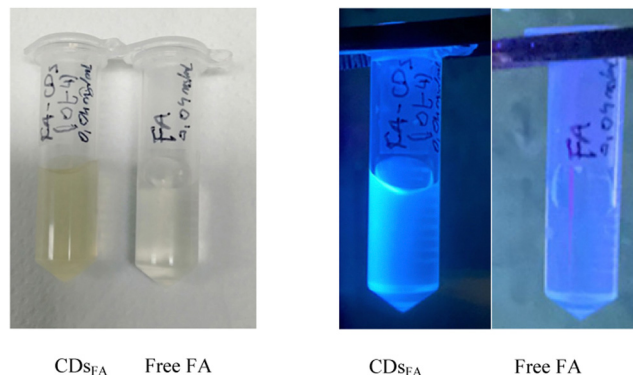

Scheme 1 Schematic of CDs_{FA} synthesis.

Fig. 1 Solutions of free FA and CDs$_{FA}$ in Milli-Q water at 40 µg mL^{-1} under white light (left) and under UV irradiation at 365 nm (right).
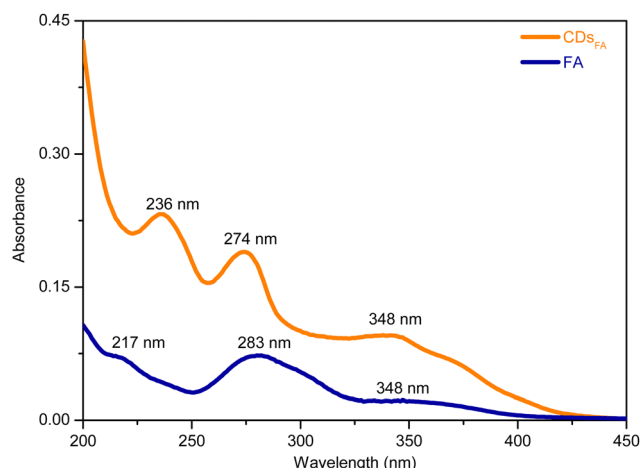

Fig. 2 UV-visible absorption spectra of FA (10 µg mL^{-1} in Milli-Q water, blue curve) and CDs$_{FA}$ (10 µg mL^{-1} in Milli-Q water, orange curve).

(ii) CDs$_{FA}$ would appear to be particles with a core of carbon (major) with a very weak nitrogen doping, since oxygen was not identified by the EELS measurements, (iii) these cores are, for sure, decorated by organic N and/or O based hydrocarbon groups, as suggested by XPS and FTIR, (iv) the particles are non-crystalline, according to TEM observations, and (v) are very probably not FA-based polymers, since their core composition does not include oxygen whereas FA contains both N and O heteroatoms in almost the same atomic ratio.

The photoluminescent properties of CDs$_{FA}$

The optical properties of the CDs$_{FA}$ were characterized by recording the UV-visible absorption (Fig. 2) and emission (Fig. 3) spectra of their aqueous solutions and comparing them to those of free FA. Interestingly, the spectra of both CDs$_{FA}$ and FA present π–π* sp^2 carbon UV bands (274 and 283 nm, respectively) with a shoulder attributed to an n–π* transition of a carbonyl function (348 nm), suggesting structural analogies between FA and at least the surface of CDs$_{FA}$. This also demonstrates that some UV chromophoric organic groups are present in both systems.

Their optical photoluminescence (PL) response was recorded by exciting them at a wavelength increasing from 300 to 410 nm (Fig. 3a). CDs$_{FA}$ are luminescent, with two main emissions, a stronger one at around 450 nm, corresponding to the blue-green emission observed (Fig. 1) under UV excitation, and a weaker one around 500 nm, assumed to be due to the water Raman signature. Interestingly, whereas FA, as an organic chromophore, requires excitation at a wavelength close to the LUMO–HOMO transition energy involved and relaxes radiatively at a constant energy, slightly smaller than the excitation one, CDs$_{FA}$ can be excited over a wider range of wavelengths, as long as the corresponding energies remain higher than those required for the excitation of the involved emitting surface state levels within the semiconducting core band gap of CDs, as already reported in several works dealing with CDs photoluminescence (Fig. 3b).[19]

The photoluminescence quantum yield of CDs$_{FA}$ (Φ_{CD}) was then computed using the equation below and quinine sulfate monohydrate (SQ), dissolved in 0.1 M sulfuric acid, as a reference. It expresses the ability of an excited chemical system to emit a photon.

$$\Phi_{CD} = \frac{\dfrac{I_{CD}\left(1 - 10^{-A_{CD}}\right)}{I_{SQ}\left(1 - 10^{-A_{SQ}}\right)} \times n^2}{n_{H_2SO_4}{}^2} \times \Phi_{SQ}$$
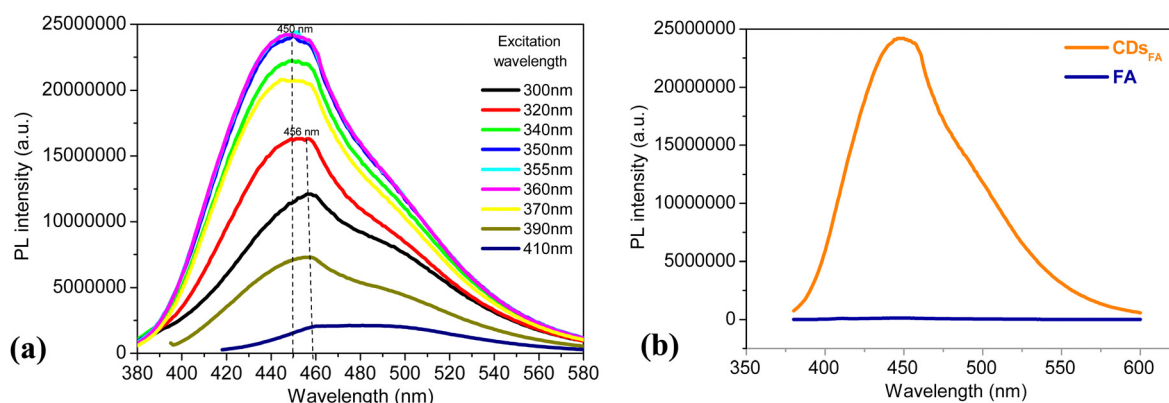

Fig. 3 (a) Photoluminescence (PL) emission spectra of CDs$_{FA}$ recorded at different excitation wavelengths (10 µg mL^{-1} in Milli-Q water). (b) Photoluminescence (PL) emission spectra of FA and CDs$_{FA}$ recorded after an excitation at 360 nm (10 µg mL^{-1} in Milli-Q water).

This journal is © the Owner Societies 2023

Phys. Chem. Chem. Phys., 2023, **25**, 14324–14333 | **14327**

where $\Phi_{SQ} = 0.54$ is the value of the SQ fluorescence quantum yield, $n = 1$, the refractive index of water and $n_{H_2SO_4} = 1.3391$, the refractive index of H_2SO_4 0.1 M, I, the intensity of photoluminescence band of CDs_{FA} (I_{CD}) or SQ (I_{SQ}) and, A, the corresponding absorbance value of CDs_{FA} (A_{CD}) and SQ (A_{SQ}), at their corresponding excitation wavelength.

A quantum yield of $39 \pm 2\%$ was thus obtained for excitation wavelengths ranging from 300 to 370 nm (Table S1 in the ESI†). These values are significantly greater than that reported by Bhunia *et al.* (9% at 365 nm).[42] This difference may be explained by an improved purification process providing CDs_{FA}.

CDs_{FA}/FA-R interaction study

FA-R are cell membrane-associated proteins responsible for FA transportation within the cells *via* a specific receptor-mediated endocytosis phenomenon.[46] Although expressed at very low levels in most tissues, FA-R are overexpressed in many cancer cells[5] and are considered to be tumour-specific target platforms. So, as explained before, folate binding protein (FBP), the soluble form of FA-R with high affinity for FA,[47] was used in this study as a surrogate of FA-R. In particular, we evaluated the interaction of CDs_{FA} with a bovine form of FBP (bFBP), isolated from cow milk.[48] The high degree of homology with the human milk FBP supports the idea that this protein can serve as an analytical tool[43] and a model in ligand–protein interaction studies.[49] Indeed, Nygren-Babol *et al.* described the interaction between folic acid and bFBP with a dissociation constant (K_d) at the pM range, using surface plasmon resonance.[50] In what follows, bFBP will be expressed as FBP.

To highlight CDs_{FA}/FBP interaction, fluorescence emission spectroscopy, which is a powerful method for detecting molecular interactions,[51] was used. We typically followed the photoluminescence (PL) intensity variation of the protein in the 320–400 nm wavelength range after excitation at 280 nm while varying the concentration of the ligand (FA or CDs_{FA}). First, to validate our method, we determined the dissociation constant (K_d) for the interaction between FBP and FA (see ESI†). The value of K_d obtained, $(9.2 \pm 0.3) \times 10^{-8}$ M, enables the quantification of this phenomenon and confirms that FA binds efficiently to FBP under our experimental conditions.

In a second step, we transposed this method to study CDs_{FA}/FBP interaction, which can be defined as follows:
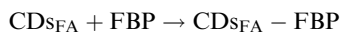
$$CDs_{FA} + FBP \rightarrow CDs_{FA} - FBP$$

with

$$K_d = \frac{[CDs_{FA}][FBP]}{[CDs_{FA} - FBP]} \tag{1}$$

Adding CDs_{FA} to a solution of FBP leads to a quenching of the fluorescence intensity and a 2 nm red shift (Fig. 4). Moreover, the experimental spectrum of FBP in the presence of CDs_{FA} is different from that of theoretical sum of the FBP and CDs_{FA} spectra, indicating an interaction between the two components. Furthermore, the titration of FBP by CDs_{FA} (Fig. 5) shows a decrease in the fluorescence intensity at an emission
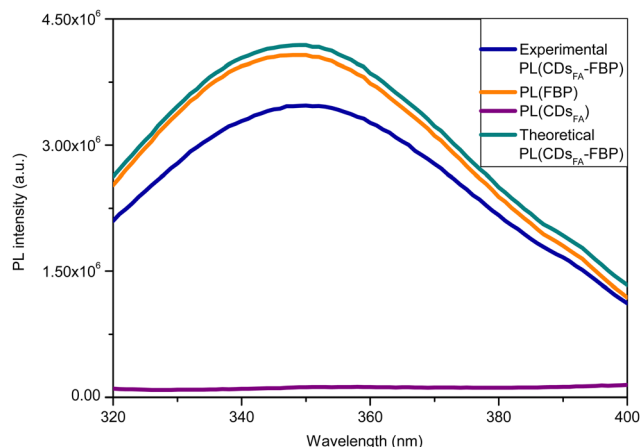

Fig. 4 Emission spectra of CDs_{FA} (purple), FBP (orange) and FBP in the presence of CDs_{FA} (CDs_{FA}-FBP; blue) and the theoretical sum of photoluminescence (PL) intensity of CDs_{FA} and FBP (CDs_{FA}-FBP; cyan). experimental conditions: [FBP] = 0.5 μm and [CDs_{FA}] = 2 μg ml^{-1} in 20 mM phosphate buffer, pH 7.4 at 25 °C. λ_{exc} = 280 nm.
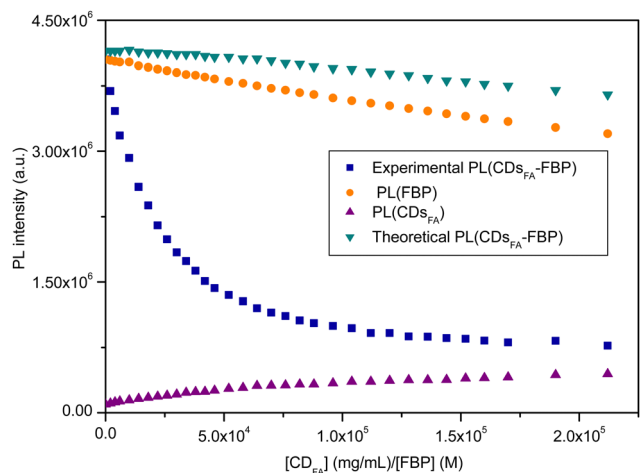

Fig. 5 Photoluminescence (PL) variations at 351 nm of CDs_{FA} (purple), FBP (orange), FBP in the presence of CDs_{FA} (blue) and the theoretical sum of PL intensity of CDs_{FA} and FBP (green) as a function of [CDs_{FA}]/[FBP] ratio. λ_{exc} = 280 nm.

wavelength of 351 nm, similar to that for FA/FBP interaction (Fig. S7 in the ESI†). We therefore observed that CDs_{FA} bind to FBP with high affinity.

The reverse experiment, *i.e.* the addition of a solution of FBP to CDs_{FA} in solution, was set up to evaluate the influence of such addition on the PL properties of the NPs. We observed an exaltation of these PL properties when the nanoparticles were excited at 350 nm (Fig. S9 and S10 in the ESI†).

Ideally, to fully characterise this interaction, the constant K_d is calculated and compared to that associated with free FA. The molecular weight of CDs_{FA} is required. An attempt was made to obtain a value by high resolution mass spectroscopy (HRMS). Electrospray ionisation (ESI†) results are presented in the ESI† (Fig. S11). Unfortunately, they only demonstrate that folic acid
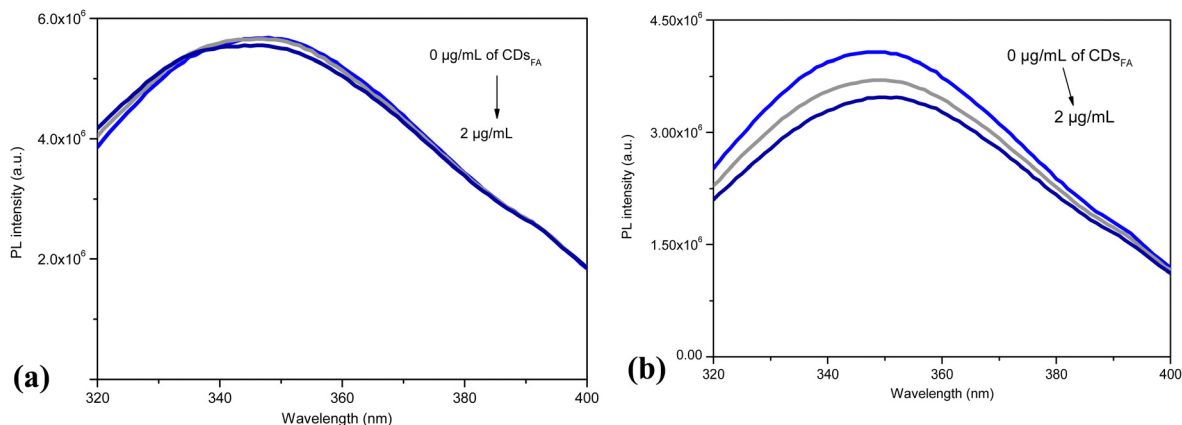
14328 | *Phys. Chem. Chem. Phys.*, 2023, **25**, 14324–14333

This journal is © the Owner Societies 2023

Fig. 6 (a) Lactoferrin (LF) (b) FBP phospholuminescence (PL) emission spectra upon addition of increasing amounts of CDs$_{FA}$. Experimental conditions: [LF] = [FBP] = 0.5 μM in a phosphate buffer 20 mM, pH 7.4 at 25 °C. The CDs$_{FA}$ concentration varied from 0 to 2 μg mL^{-1}. λ_{exc} = 280 nm.

residues are the main components of this sample. This is an important piece of information for our purpose, but they do not allow any determination of the total molecular weight of our nano-objects. Attempts to determine nanoparticle molecular

weights by HRMS have already been described with more or less success. For instance, Hou *et al.* prepared antibacterial carbon dots from ciprofloxacin and carried out laser desorption/ionization time-of-flight mass spectroscopy, but only ciprofloxacin fragments could be identified.[52]
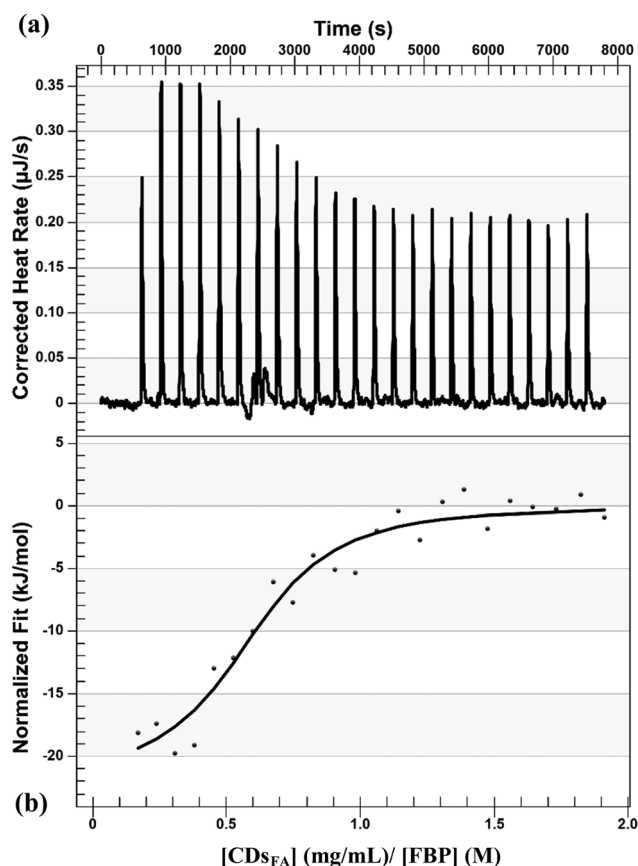

Fig. 7 ITC thermogram resulting from titrating CDs$_{FA}$ suspension (0.11 mg mL^{-1}, phosphate buffer pH 7.4, 2 μL injections) into a FBP solution at 25 °C (20 μM, phosphate buffer pH 7.4) exhibits exothermic peaks. (a) Raw data resulting from titrating CDs$_{FA}$ suspension into a FBP solution; (b) thermogram fitted with an independent binding model (straight line) demonstrates a negative enthalpy change (Δ*H*). The direct titration experiments were performed in triplicate.
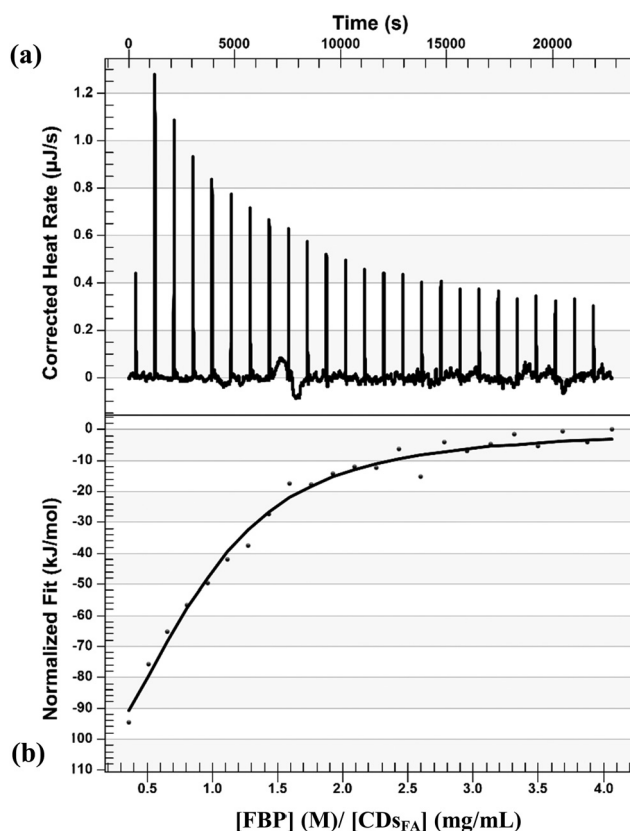

Fig. 8 ITC thermogram resulting from titrating FBP solution (100 μM, phosphate buffer pH 7.4, 2 μL injections) into a CDs$_{FA}$ suspension at 25 °C (8.55 μg mL^{-1}, phosphate buffer pH 7.4) exhibits exothermic peaks. (a) Raw data resulting from titrating FBP solution into a CDs$_{FA}$ suspension; (b) thermogram fitted with an independent binding model (straight line) demonstrates a negative enthalpy change (Δ*H*). The reverse titration experiments were performed in duplicate.

This journal is © the Owner Societies 2023

Phys. Chem. Chem. Phys., 2023, **25**, 14324–14333 | **14329**

The same experimental strategy was applied to appreciate, at least qualitatively, the selectivity of this interaction using lactoferrin (LF), which is not the natural FA receptor even if it is capable of binding it.[44]

LF is a glycoprotein of the transferrin family initially described as an iron-binding molecule, but it is now known to be a multifunctional protein.[53] Tavares *et al.* investigated the ability of positively charged LF to form complexes with negatively charged FA at pH 5.5, and found a moderate binding constant K_a of 10^5 M^{-1}.[44] Following the previously described methodology, we added increasing amounts of CDs_{FA} to a solution of LF, measured the corresponding fluorescence emission and plot curves presented in Fig. 6a. As expected, the addition of increasing amounts of NPs does not modify the fluorescence emission spectrum of LF, expressed as PL intensity, demonstrating that the interaction is weak compared to that observed when CDs_{FA} are added to a solution of FBP, under the same conditions of concentration, pH and temperature (Fig. 6b). Furthermore, no spectral changes are observed for either LF or the corresponding putative complex when the FI

is expressed as a function of the emission wavelength, in accordance with the absence of a strong interaction between these both partners (Fig. S12 in ESI†).

To reinforce the complex formation observed during the spectrofluorimetric study between FBP and CDs_{FA}, we employed isothermal titration calorimetric (ITC). ITC usually provides enthalpy (ΔH) and entropy (ΔS) parameters of the binding reaction but also the corresponding dissociation constant (K_d) and the stoichiometry (n) of the complex. Taking into account the previous limitations we met (no molecular weight determination), only a qualitative study was set up. Our experimental data are presented in Fig. 7–9 and were fitted with an independent-site model. Ligands (CDs_{FA}) and macromolecules (FBP or lactoferrin) were placed in the same buffer to avoid large background heat effects related to the ligand injection into the buffer. These background heats were measured in an experiment wherein the ligand is injected into a buffer (Fig. 9).

ITC is a classical method that intrinsically measures the heat produced (or consumed) when components are interact together, including during protein–nanoparticle interaction.[54]
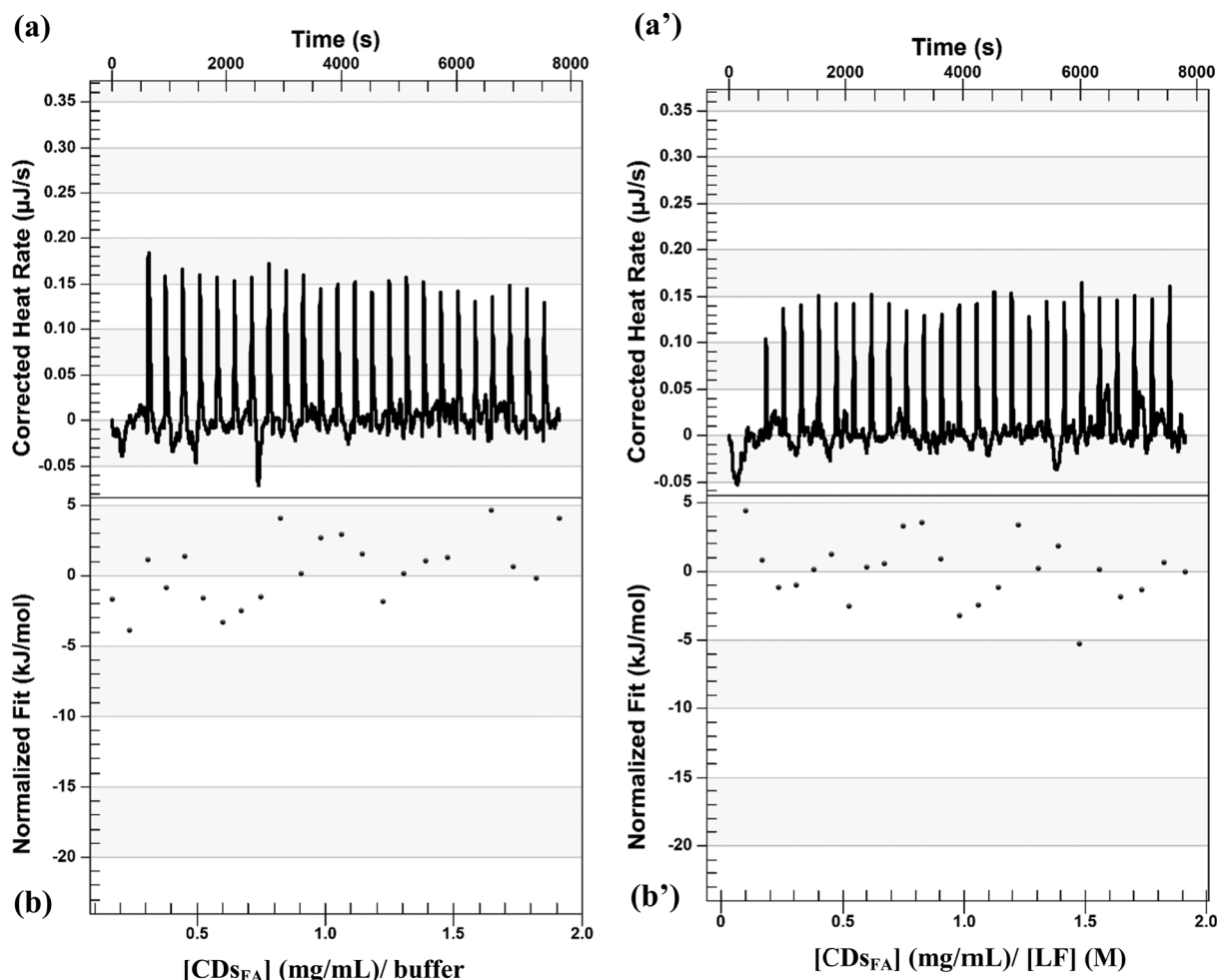

Fig. 9 (a and a′) ITC thermogram resulting from titrating CDs_{FA} suspension (0.11 mg mL^{-1}, phosphate buffer pH 7.4, 2 μL injections) into a lactoferrin (right) or phosphate buffer (left) solution at 25 °C (20 μM, phosphate buffer pH 7.4) exhibits exothermic peaks; and (b and b′) show the integrated data of the thermogram values.

14330 | *Phys. Chem. Chem. Phys.*, 2023, **25**, 14324–14333

This journal is © the Owner Societies 2023

In our conditions, the addition of a solution of CDs_{FA} to a solution of FBP (direct titration) led to heat production as presented in Fig. 7, where raw data are presented as a series of peaks measured as power ($\mu J\ s^{-1}$) *versus* time. The formation of the CDs_{FA}/FBP complex was further confirmed by the reverse ITC titrations, given in Fig. 8, where a solution of FBP was added to CDs_{FA} in solution. In both experiments, the plot of heat as a function of [ligand]/[macromolecule] ratio provided a sigmoidal curve, indicating a single binding event, demonstrated that binding reactions proceed spontaneously as they are thermodynamically favoured, and confirming the interaction previously observed. The direct and reverse reactions are exothermic ($\Delta H < 0$, Fig. 7 and 8), as also observed during the titration of CDots by HSA or BSA.[55] Moreover, as most of the protein–Np interactions are enthalpy-driven ($|\Delta H| < |T\Delta S|$), we then suggest that the main driving force of the interaction between FBP and the NPs is non-covalent bonding, as van der Waals and/or hydrogen interactions.[56] Furthermore, the CDs_{FA} are negatively charged whereas the FBP is positively charged at pH 7, regarding its isoelectric point (pI) value around 8, electrostatic bonds may also contribute to the exothermic reaction.

ITC was also used to study a putative protein selectivity. At pH 7.4, the thermogram profiles of the titration of lactoferrin by CDs_{FA} shows a weak heat production (Fig. 9, right) which is similar to the one observed when CDs_{FA} in solution are added to the buffer (Fig. 9, left), demonstrating the absence of interaction between this protein and the particles in these experimental conditions.

Recently Jin *et al.* suggested an explanation of the interaction between hydrothermally FA-made CDs and cells overexpressing FA-R.[57] They explained that the pterin moiety, also presents in FA's structure, and required to the interaction with the FA-R, is maintained in the produced CDs. Hence, they showed that structural similarities exist between their NPs and FA using UV-visible, PL, FT-IR, XPS and NMR data. We also observed them (see the ESI†), even if the structural properties of CDs_{FA} do not completely match with those of Jin *et al.*'s particles. Indeed, certain differences can, however, be evidenced between the two set of particles and are certainly related to differences in the operating synthesis conditions (FA concentration, NaOH addition, reaction temperature and so one). Despite these discrepancies, all the CDs obtained from FA bind efficiently to their target demonstrating an important tolerance in their structure. The latter is certainly linked to the previously described tolerance of FA to structural modifications.

Conclusions

Thus, the literature describes a very large variety, in nature and size, of objects capable of being recognized by the FA-R; among these are CDs_{FA}. Several publications, cited in the introduction of this article, demonstrate the capacity of these objects to target FA-R in a cellular medium. The present study is the first to verify this interaction in a direct manner, bringing together the main actors of this interaction in a cell-free system.

For this purpose, we synthesised carbon dots from folic acid, as a source of carbon, and characterised them. Using a folate-binding protein, a soluble form of the folic acid receptor with a high affinity for folic acid, its natural ligand, we established the formation of a complex between the two partners and the selectivity of this interaction. To our knowledge, these objects have only been used to visualize cancerous cells. The demonstration of their direct interaction with their target contributes to extending their field of application. Indeed, the possible drug delivery of an anti-cancer compound, for instance, that would have been grafted to them becomes possible.

Author contributions

Erika Adhel: investigation, formal analysis, validation, data curation, writing—review and editing, visualization; Nguyêt-Thanh Ha Duong: conceptualization, methodology, formal analysis, validation, resources, data curation, writing—review and editing, funding acquisition, visualization; Thi Huyen Vu: investigation, formal analysis, validation, data curation, visualization; Dario Taverna: investigation, formal analysis, resources, validation, data curation, funding acquisition, visualization; Souad Ammar: formal analysis, writing—review and editing, funding acquisition, visualization and Nawal Serradji: conceptualization, methodology, formal analysis, resources, data curation, writing—original draft preparation, writing—review and editing, supervision, project administration, funding acquisition, visualization. All authors have read and agreed to the published version of the manuscript.

Conflicts of interest

The authors declare no conflicts of interest.

Acknowledgements

References

1 V. Schirrmacher, From chemotherapy to biological therapy: A review of novel concepts to reduce the side effects of

This journal is © the Owner Societies 2023

Phys. Chem. Chem. Phys., 2023, **25**, 14324–14333 | **14331**

systemic cancer treatment (Review), *Int. J. Oncol.*, 2019, **54**, 407–419.

2 S. Kwiatkowski, B. Knap, D. Przystupski, J. Saczko, E. Kędzierska, K. Knap-Czop, J. Kotlińska, O. Michel, K. Kotowski and J. Kulbacka, Photodynamic therapy – mechanisms, photosensitizers and combinations, *Biomed. Pharmacother.*, 2018, **106**, 1098–1107.

3 R. Abdollahi, S. Najafi, E. Razmpoosh, R. S. Shoormasti, S. Haghighat, M. Raji Lahiji, M. Chamari, M. Asgari, E. Cheshmazar and M. Zarrati, The Effect of Dietary Intervention Along with Nutritional Education on Reducing the Gastrointestinal Side Effects Caused by Chemotherapy Among Women with Breast Cancer, *Nutr. Cancer*, 2019, **71**, 922–930.

4 N. Parker, M. J. Turk, E. Westrick, J. D. Lewis, P. S. Low and C. P. Leamon, Folate receptor expression in carcinomas and normal tissues determined by a quantitative radioligand binding assay, *Anal. Biochem.*, 2005, **338**, 284–293.

5 Y. G. Assaraf, C. P. Leamon and J. A. Reddy, The folate receptor as a rational therapeutic target for personalized cancer treatment, *Drug Resistance Updates*, 2014, **17**, 89–95.

6 M. Scaranti, E. Cojocaru, S. Banerjee and U. Banerji, Exploiting the folate receptor alpha in oncology, *Nat. Rev. Clin. Oncol.*, 2020, **17**, 349–359.

7 W. Xia and P. S. Low, Folate-Targeted Therapies for Cancer, *J. Med. Chem.*, 2010, **53**, 6811–6824.

8 S. Raj, S. Khurana, R. Choudhari, K. K. Kesari, M. A. Kamal, N. Garg, J. Ruokolainen, B. C. Das and D. Kumar, Specific targeting cancer cells with nanoparticles and drug delivery in cancer therapy, *Semin. Cancer Biol.*, 2021, **69**, 166–177.

9 F. Yan, Z. Sun, H. Zhang, X. Sun, Y. Jiang and Z. Bai, The fluorescence mechanism of carbon dots, and methods for tuning their emission color, *Microchim. Acta*, 2019, **186**, 583.

10 X. Xu, R. Ray, Y. Gu, H. J. Ploehn, L. Gearheart, K. Raker and W. A. Scrivens, Electrophoretic Analysis and Purification of Fluorescent Single-Walled Carbon Nanotube Fragments, *J. Am. Chem. Soc.*, 2004, **126**, 12736–12737.

11 U. A. Rani, L. Y. Ng, C. Y. Ng and E. Mahmoudi, A review of carbon quantum dots and their applications in wastewater treatment, *Adv. Colloid Interface Sci.*, 2020, **278**, 102124.

12 V. K. Sharma, T. J. McDonald, M. Sohn, G. A. K. Anquandah, M. Pettine and R. Zboril, Assessment of toxicity of selenium and cadmium selenium quantum dots: A review, *Chemosphere*, 2017, **188**, 403–413.

13 S. N. Baker and G. A. Baker, Luminescent Carbon Nanodots: Emergent Nanolights, *Angew. Chem., Int. Ed.*, 2010, **49**, 6726–6744.

14 M. Havrdova, K. Hola, J. Skopalik, K. Tomankova, M. Petr, K. Cepe, K. Polakova, J. Tucek, A. B. Bourlinos and R. Zboril, Toxicity of carbon dots – Effect of surface functionalization on the cell viability, reactive oxygen species generation and cell cycle, *Carbon*, 2016, **99**, 238–248.

15 X. Tian and X. Yin, Carbon Dots, Unconventional Preparation Strategies, and Applications Beyond Photoluminescence, *Small*, 2019, **15**, 1901803.

16 J. Pardo, Z. Peng and R. Leblanc, Cancer Targeting and Drug Delivery Using Carbon-Based Quantum Dots and Nanotubes, *Molecules*, 2018, **23**, 378.

17 M. Farshbaf, S. Davaran, F. Rahimi, N. Annabi, R. Salehi and A. Akbarzadeh, Carbon quantum dots: recent progresses on synthesis, surface modification and applications, *Artif. Cells, Nanomed., Biotechnol.*, 2018, **46**, 1331–1348.

18 H. Wang, J. Bi, B.-W. Zhu and M. Tan, Multicolorful Carbon Dots for Tumor Theranostics, *Curr. Med. Chem.*, 2018, **25**, 2894–2909.

19 A. Sciortino, A. Cannizzo and F. Messina, Carbon Nanodots: A Review—From the Current Understanding of the Fundamental Photophysics to the Full Control of the Optical Response, *C*, 2018, **4**, 67.

20 F. Yuan, T. Yuan, L. Sui, Z. Wang, Z. Xi, Y. Li, X. Li, L. Fan, Z. Tan, A. Chen, M. Jin and S. Yang, Engineering triangular carbon quantum dots with unprecedented narrow bandwidth emission for multicolored LEDs, *Nat. Commun.*, 2018, **9**, 2249.

21 W. Yang, F. Liu, R. Li, X. Wang and W. Hao, Multiple Stimuli-Responsive Fluorescent Sensor from Citric Acid and 1-(2-Aminoethyl)piperazine, *ACS Appl. Mater. Interfaces*, 2018, **10**, 9123–9128.

22 S. Zhu, Y. Song, X. Zhao, J. Shao, J. Zhang and B. Yang, The photoluminescence mechanism in carbon dots (graphene quantum dots, carbon nanodots, and polymer dots): current state and future perspective, *Nano Res.*, 2015, **8**, 355–381.

23 B. Zhi, X. Yao, Y. Cui, G. Orr and C. L. Haynes, Synthesis, applications and potential photoluminescence mechanism of spectrally tunable carbon dots, *Nanoscale*, 2019, **11**, 20411–20428.

24 J. Zhang, X. Zhao, M. Xian, C. Dong and S. Shuang, Folic acid-conjugated green luminescent carbon dots as a nanoprobe for identifying folate receptor-positive cancer cells, *Talanta*, 2018, **183**, 39–47.

25 H. Saljoughi, F. Khakbaz and M. Mahani, Synthesis of folic acid conjugated photoluminescent carbon quantum dots with ultrahigh quantum yield for targeted cancer cell fluorescence imaging, *Photodiagn. Photodyn. Ther.*, 2020, **30**, 101687.

26 S. Feng, J. Pan, C. Li and Y. Zheng, Folic acid-conjugated nitrogen-doped graphene quantum dots as a fluorescent diagnostic material for MCF-7 cells, *Nanotechnology*, 2020, **31**, 135701.

27 A. Mewada, S. Pandey, M. Thakur, D. Jadhav and M. Sharon, Swarming carbon dots for folic acid mediated delivery of doxorubicin and biological imaging, *J. Mater. Chem. B*, 2014, **2**, 698–705.

28 R. Lv, G. Li, S. Lu and T. Wang, Synthesis of Multi-Functional Carbon Quantum Dots for Targeted Antitumor Therapy, *J. Fluoresc.*, 2021, **31**, 339–348.

29 B. Yang, M. Wu, S. Pang, D. Li, Y. Yang, L. Wang, Z. Li, J. Zhang and X. Yang, One-pot synthesis of folic acid modified carbonized polymer dots with red emittision for selective imaging of cancer cells, *Nanotechnology*, 2020, **31**, 475501.

30 S. Kadian, G. Manik, N. Das and P. Roy, Targeted bioimaging and sensing of folate receptor-positive cancer cells using folic acid-conjugated sulfur-doped graphene quantum dots, *Microchim. Acta*, 2020, **187**, 458.

14332 | *Phys. Chem. Chem. Phys.*, 2023, **25**, 14324–14333

This journal is © the Owner Societies 2023

31 P. Sarkar, S. Ghosh and K. Sarkar, Folic acid based carbon dot functionalized stearic acid-g-polyethyleneimine amphiphilic nanomicelle: Targeted drug delivery and imaging for triple negative breast cancer, *Colloids Surf., B*, 2021, **197**, 111382.

32 A. Nasrin, M. Hassan and V. G. Gomes, Two-photon active nucleus-targeting carbon dots: enhanced ROS generation and photodynamic therapy for oral cancer, *Nanoscale*, 2020, **12**, 20598–20603.

33 R. V. Goreham, K. L. Schroeder, A. Holmes, S. J. Bradley and T. Nann, Demonstration of the lack of cytotoxicity of unmodified and folic acid modified graphene oxide quantum dots, and their application to fluorescence lifetime imaging of HaCaT cells, *Microchim. Acta*, 2018, **185**, 128.

34 R. I. Pinhassi, Y. G. Assaraf, S. Farber, M. Stark, D. Ickowicz, S. Drori, A. J. Domb and Y. D. Livney, Arabinogalactan−Folic Acid−Drug Conjugate for Targeted Delivery and Target-Activated Release of Anticancer Drugs to Folate Receptor-Overexpressing Cells, *Biomacromolecules*, 2010, **11**, 294–303.

35 Y. Sun, Y. Zhao, S. Teng, F. Hao, H. Zhang, F. Meng, X. Zhao, X. Zheng, Y. Bi, Y. Yao, R. J. Lee and L. Teng, Folic acid receptor-targeted human serum albumin nanoparticle formulation of cabazitaxel for tumor therapy, *Int. J. Nanomed.*, 2018, **14**, 135–148.

36 A. Narmani, M. Rezvani, B. Farhood, P. Darkhor, J. Mohammadnejad, B. Amini, S. Refahi and N. Abdi Goushbolagh, Folic acid functionalized nanoparticles as pharmaceutical carriers in drug delivery systems, *Drug Dev. Res.*, 2019, **80**, 404–424.

37 O. Yücel, A. Sengelen, S. Emik, E. Önay-Uçar, N. Arda and G. Gürdağ, Folic acid-modified methotrexate-conjugated gold nanoparticles as nano-sized trojans for drug delivery to folate receptor-positive cancer cells, *Nanotechnology*, 2020, **31**, 355101.

38 K. Butzbach, M. Konhäuser, M. Fach, D. Bamberger, B. Breitenbach, B. Epe and P. Wich, Receptor-mediated Uptake of Folic Acid-functionalized Dextran Nanoparticles for Applications in Photodynamic Therapy, *Polymers*, 2019, **11**, 896.

39 W. Guan, W. Gu, L. Ye, C. Guo, S. Su, P. Xu and M. Xue, Microwave-assisted polyol synthesis of carbon nitride dots from folic acid for cell imaging, *Int. J. Nanomed.*, 2014, **9**, 5071–5078.

40 H. Liu, Z. Li, Y. Sun, X. Geng, Y. Hu, H. Meng, J. Ge and L. Qu, Synthesis of Luminescent Carbon Dots with Ultrahigh Quantum Yield and Inherent Folate Receptor-Positive Cancer Cell Targetability, *Sci. Rep.*, 2018, **8**, 1086.

41 M. Z. Fahmi, N. F. Sholihah, A. Wibrianto, S. C. W. Sakti, F. Firdaus and J. Chang, Simple and fast design of folic acid-based carbon dots as theranostic agent and its drug release aspect, *Mater. Chem. Phys.*, 2021, **267**, 124596.

42 S. K. Bhunia, A. R. Maity, S. Nandi, D. Stepensky and R. Jelinek, Imaging Cancer Cells Expressing the Folate Receptor with Carbon Dots Produced from Folic Acid, *ChemBioChem*, 2016, **17**, 614–619.

43 L. Nygren-Babol and M. Jägerstad, Folate-Binding Protein in Milk: A Review of Biochemistry, Physiology, and Analytical Methods, *Food Sci. Nutr.*, 2012, **52**, 410–425.

44 G. M. Tavares, T. Croguennec, S. Lê, O. Lerideau, P. Hamon, A. F. Carvalho and S. Bouhallab, Binding of Folic Acid Induces Specific Self-Aggregation of Lactoferrin: Thermodynamic Characterization, *Langmuir*, 2015, **31**, 12481–12488.

45 I. Aprodu, L. Dumitrascu, G. Râpeanu, G.-E. Bahrim and N. Stănciuc, Spectroscopic and Molecular Modeling Investigation on the Interaction between Folic Acid and Bovine Lactoferrin from Encapsulation Perspectives, *Foods*, 2020, **9**, 744.

46 M. J. Turk, G. J. Breur, W. R. Widmer, C. M. Paulos, L.-C. Xu, L. A. Grote and P. S. Low, Folate-targeted imaging of activated macrophages in rats with adjuvant-induced arthritis, *Arthritis Rheum.*, 2002, **46**, 1947–1955.

47 H. Gary, Folate-binding proteins, *Annu. Rev. Nutr.*, 1990, **10**, 319.

48 J. Holm, S. I. Hansen and M. Høier-Madsen, Ionic Charge, Hydrophobicity and Tryptophan Fluorescence of the Folate Binding Protein Isolated from Cow's Milk, *Biosci. Rep.*, 2001, **21**, 305–313.

49 I. Svendsen, S. I. Hansen, J. Holm and J. Lyngbye, The complete amino acid sequence of the folate-binding protein from cow's milk, *Carlsberg Res. Commun.*, 1984, **49**, 123–131.

50 L. Nygren-Babol, Å. Sternesjö, M. Jägerstad and L. Björck, Affinity and Rate Constants for Interactions of Bovine Folate-Binding Protein and Folate Derivatives Determined by Optical Biosensor Technology. Effect of Stereoselectivity, *J. Agric. Food Chem.*, 2005, **53**, 5473–5478.

51 S. Deshayes and G. Divita, Fluorescence Technologies for Monitoring Interactions Between Biological Molecules In Vitro, *Prog. Mol. Biol. Transl. Sci.*, 2013, **113**, 109–143.

52 P. Hou, T. Yang, H. Liu, Y. F. Li and C. Z. Huang, An active structure preservation method for developing functional graphitic carbon dots as an effective antibacterial agent and a sensitive pH and Al(III) nanosensor, *Nanoscale*, 2017, **9**, 17334–17341.

53 G.-M. Isui Abril, C. Tania Siqueiros, A.-G. Sigifredo and R.-C. Quintín, Lactoferrin a multiple bioactive protein: an overview, *Biochim. Biophys. Acta*, 2012, **1820**, 226–236.

54 D. Prozeller, S. Morsbach and K. Landfester, Isothermal titration calorimetry as a complementary method for investigating nanoparticle–protein interactions, *Nanoscale*, 2019, **11**, 19265–19273.

55 S. Mandal, M. Hossain, P. S. Devi, G. S. Kumar and K. Chaudhuri, Interaction of carbon nanoparticles to serum albumin: elucidation of the extent of perturbation of serum albumin conformations and thermodynamical parameters, *J. Hazard. Mater.*, 2013, **248–249**, 238–245.

56 R. Huang and B. L. T. Lau, Biomolecule–nanoparticle interactions: Elucidation of the thermodynamics by isothermal titration calorimetry, *Biochim. Biophys. Acta, Gen. Subj.*, 1860, **2016**, 945–956.

57 Y. Jin, Q. Zhang, X. Qin, Z. Liu, Z. Li, X. Zhong, L. Xia, J. He and B. Fang, Carbon dots derived from folic acid attenuates osteoarthritis by protecting chondrocytes through NF-κB/MAPK pathway and reprogramming macrophages, *J. Nanobiotechnol.*, 2022, **20**, 469.

This journal is © the Owner Societies 2023

Phys. Chem. Chem. Phys., 2023, **25**, 14324–14333 | **14333**